

## Supplementary Materials for **Direct 4D printing via active composite materials**

Zhen Ding, Chao Yuan, Xirui Peng, Tiejun Wang, H. Jerry Qi, Martin L. Dunn

Published 12 April 2017, *Sci. Adv.* **3**, e1602890 (2017)  
DOI: 10.1126/sciadv.1602890

### **This PDF file includes:**

- section S1. Thermomechanical properties of polymers
- section S2. Additional results
- section S3. Geometry of printed samples
- section S4. Modeling and simulation
- fig. S1. Thermomechanical properties of elastomer (TangoBlack+) and glassy polymer SMP (VeroClear) as determined by DMA.
- fig. S2. Contribution in overall curvature from CTE mismatch strain and built-in compressive strain.
- fig. S3. A lattice structure (dimensions in mm) printed in an open configuration and then deployed into a compact configuration upon heating.
- fig. S4. Design of the printed sample in Fig. 3A.
- fig. S5. Design of the printed sample in Fig. 3B.
- fig. S6. Design of the printed sample in Fig. 3C.
- fig. S7. Design of the printed sample in Fig. 4A.
- fig. S8. Design of the printed sample in Fig. 4B.
- fig. S9. Design of the printed sample in Fig. 4C.
- fig. S10. Design of the printed sample in fig. S3.
- table S1. List of parameters for constitutive model.

## section S1. Thermomechanical properties of polymers

We measured the storage modulus, tan delta, and thermal strain versus temperature of both the SMP and the elastomer. These results were obtained with a layer printing time of 68s, but differ insignificantly from results with different printing times. Upon heating the storage modulus of Veroclear decreases slightly until  $\sim 40^{\circ}\text{C}$  above which it reduces dramatically. In contrast, the decrease of TangoBlack+' storage modulus has basically ceased after  $10^{\circ}\text{C}$  (fig. S1A). The peak of tan delta in fig. S1B indicates the glass transition temperature ( $T_g$ )  $\sim 62^{\circ}\text{C}$  and  $\sim 8^{\circ}\text{C}$  for Veroclear and TangoBlack+, respectively. TangoBlack+ has an almost linear thermal strain  $\sim 1\%$  from room temperature ( $25^{\circ}\text{C}$ ) to  $80^{\circ}\text{C}$ , while it is  $\sim 0.8\%$  for Veroclear and nonlinear indicating a phase transition in that temperature range. The mismatch thermal strain between Veroclear and TangoBlack+ is less than  $0.2\%$  in the measured temperature range. The residual thermal strains of both Veroclear and TangoBlack+ are almost zero after they were cooled back to room temperature in a heating-cooling cycle.

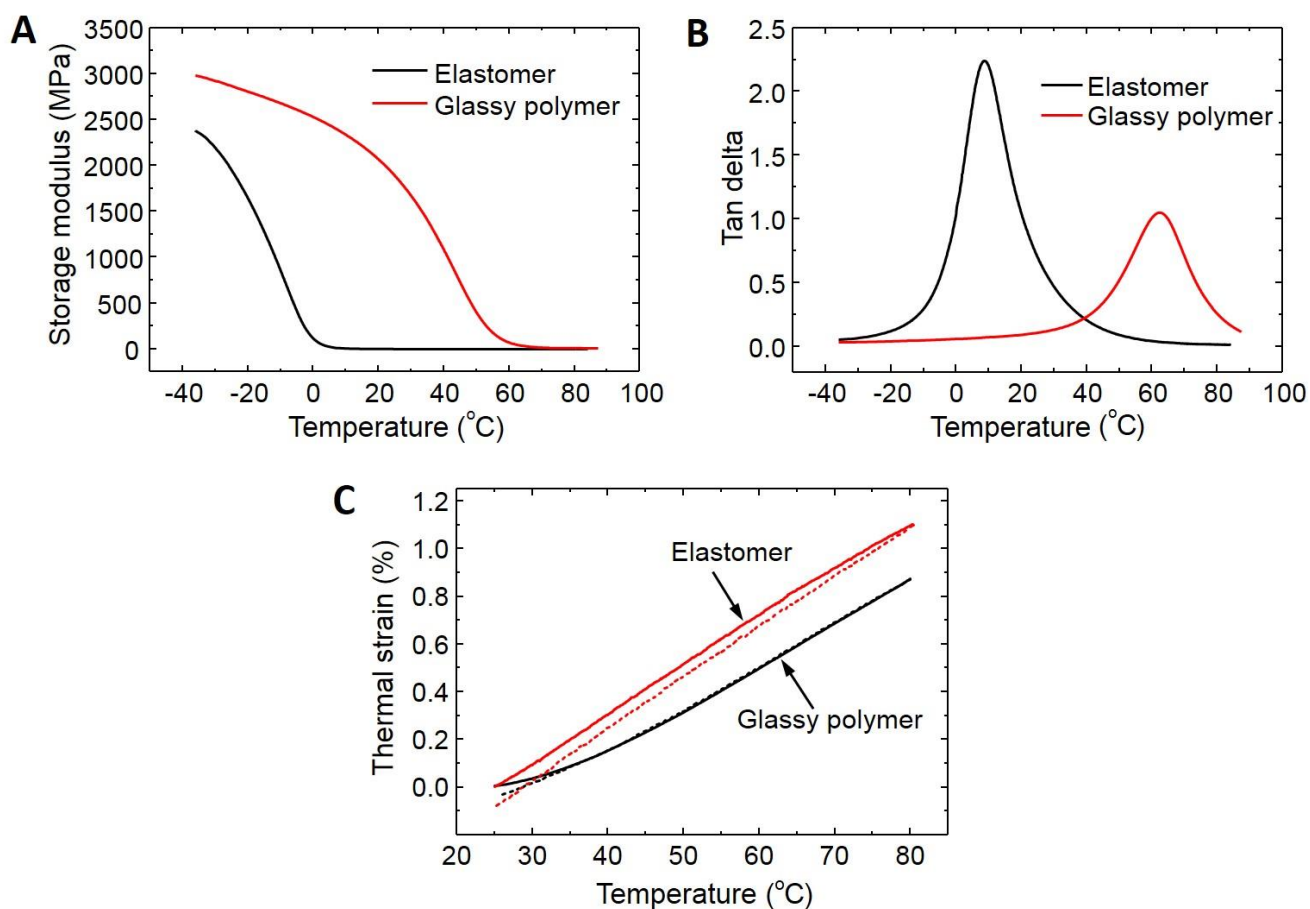


**fig. S1. Thermomechanical properties of elastomer (TangoBlack+) and glassy polymer SMP (VeroClear) as determined by DMA.** (A) Storage modulus versus temperature; (B) Tan delta versus temperature; (C) Thermal strain in one heating (solid lines) and cooling (dash lines) cycle.

## section S2. Additional results

We quantify the ratio between the built-in compressive strain and CTE mismatch strain towards bending curvature. The CTE mismatch also contributes to the overall bending, but to a lesser extent, especially with the longer layer printing time.

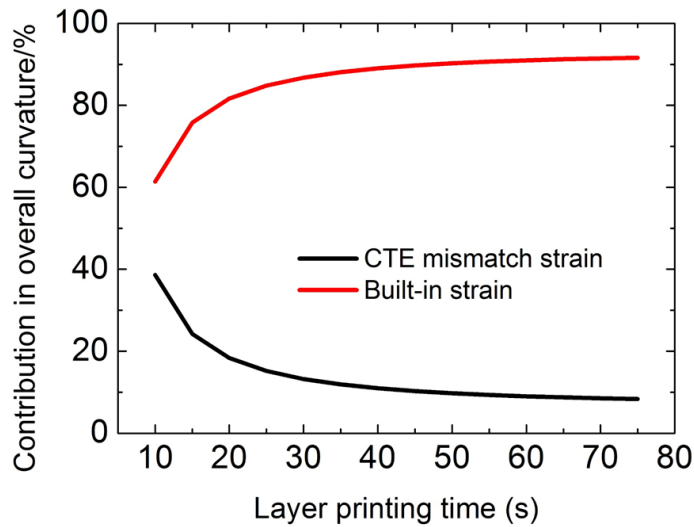


**fig. S2. Contribution in overall curvature from CTE mismatch strain and built-in compressive strain.**

Various shape actuations can be achieved via our direct 4d printing approach by carefully configuring materials in structure. Opposite to Fig. 4A, where the printed collapsed lattice structure deploys into an open configuration upon heating, a printed open lattice structure here dramatically collapses into a compact one with a structural compression of ~62% and a lateral contraction of ~6% upon heating. Finite element simulations (the pic at the right bottom of fig. S2) show good agreement with a predicted compression of 64% and lateral contraction of 7%.

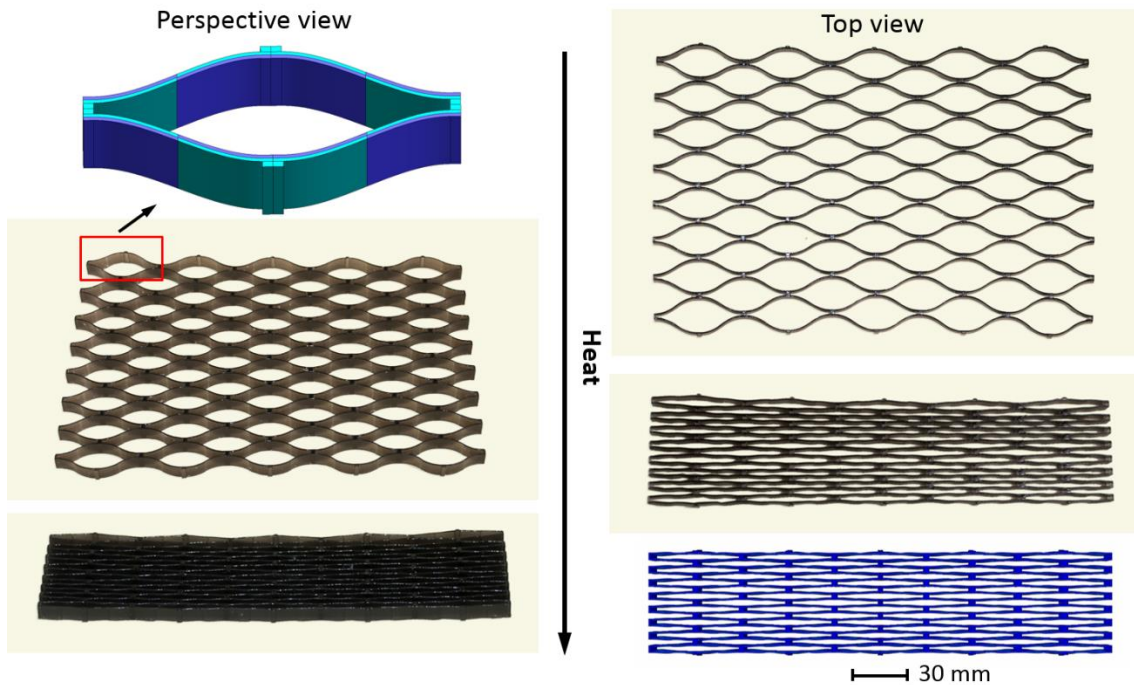


**fig. S3. A lattice structure (dimensions in mm) printed in an open configuration and then deployed into a compact configuration upon heating.** The structure has a size of 180 mm×119 mm×7 mm and a SMP/elastomer bilayer thicknesses of 0.4/0.4 mm.



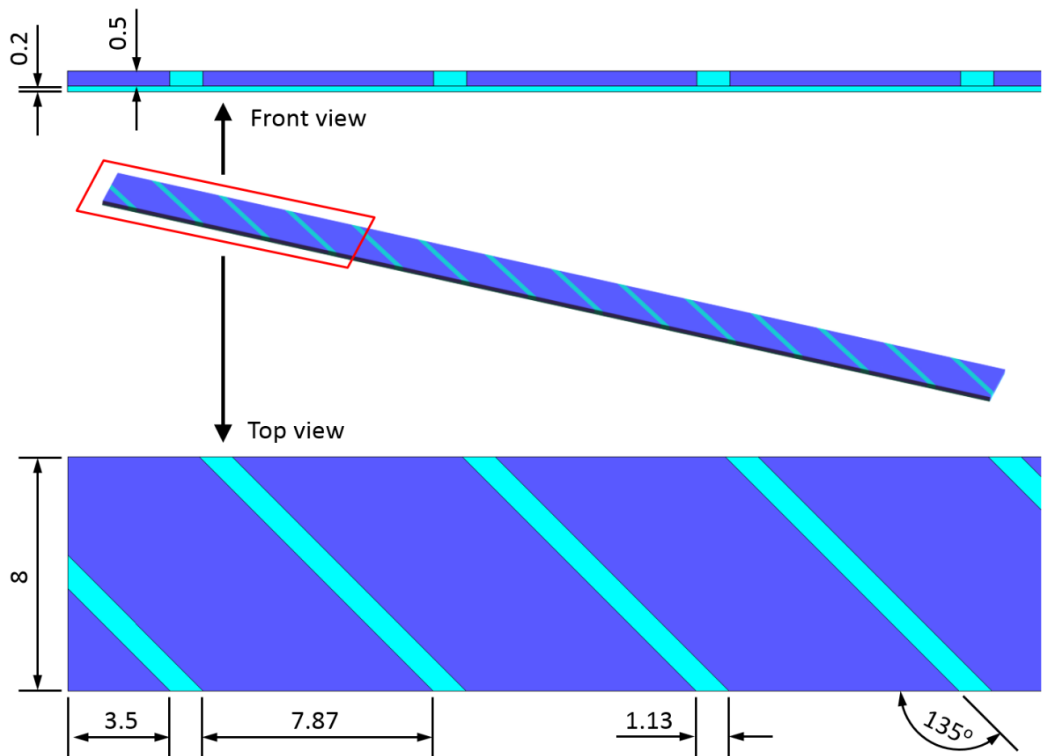


**fig. S5.** Design of the printed sample in Fig. 3B. Two-layer flat strips of 128 mm × 8 mm × 0.7 mm with Veroclear/Tangoblack+ thicknesses of 0.2/0.5 mm and an SMP separator is oriented at 45° fabricated with a layer printing time of 68 s and a total printing time of 70 min.

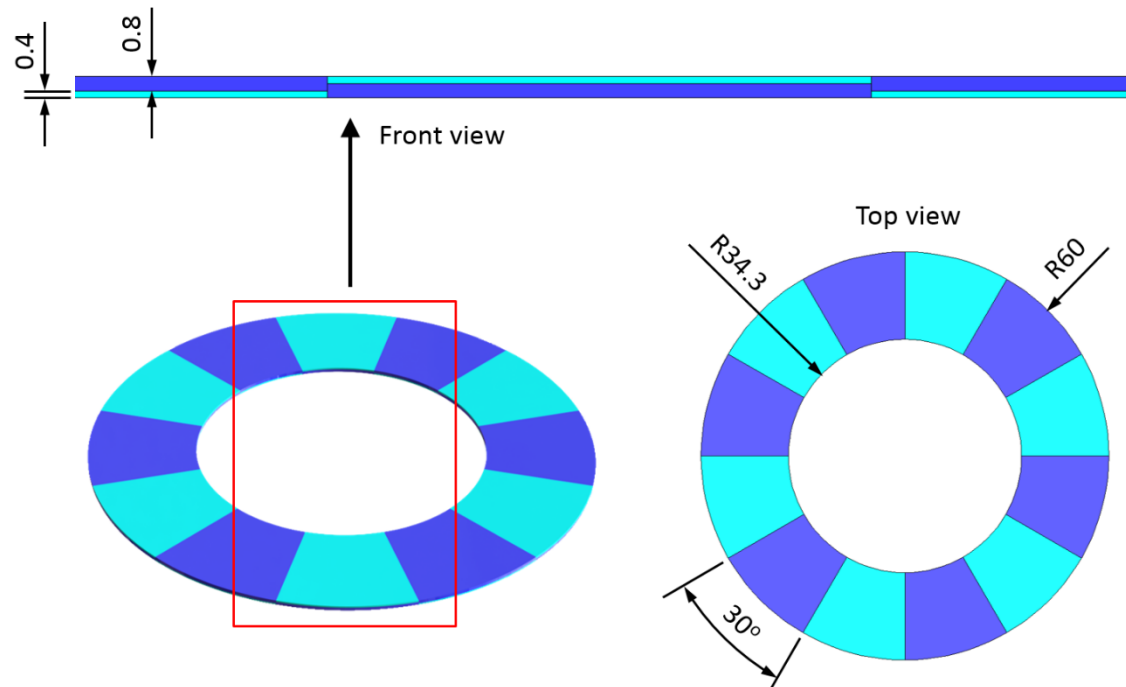


**fig. S6.** Design of the printed sample in Fig. 3C. Two-layer flat rings of 120/68.6-mm outer/inner diameter and 1.2-mm thickness, where Veroclear/Tangoblack+ has thicknesses of 0.4/0.8 mm and alternates along the circumference, fabricated with a layer printing time of 68 s and a total printing time of 89 min.

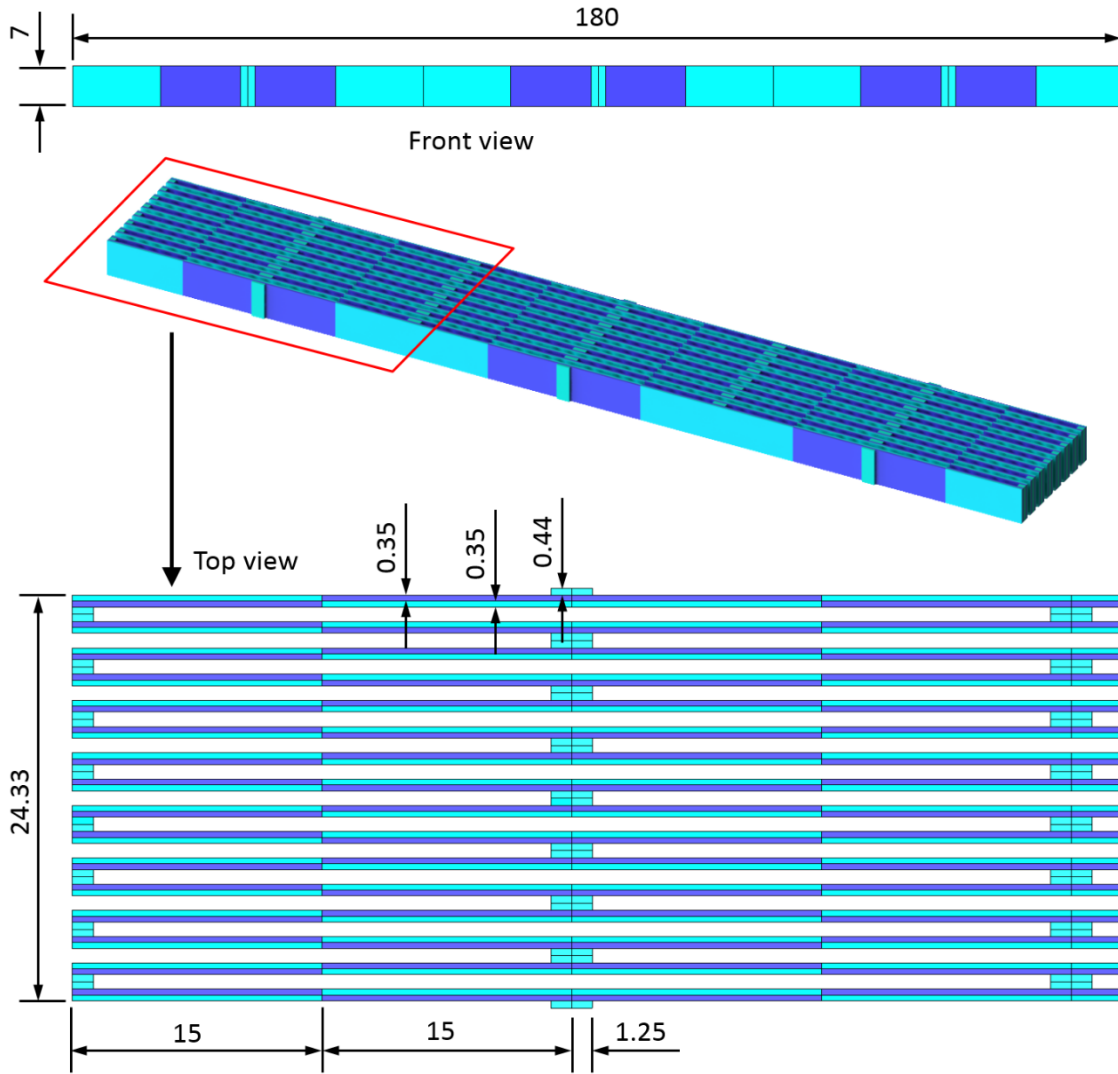


**fig. S7. Design of the printed sample in Fig. 4A.** Closed lattice with an overall size of 180 mm × 25.2 mm × 7 mm. Veroclear/Tangoblack+ (0.35/0.35 mm) bilayers are printed perpendicular to the build tray and fabricated with a layer printing time of 68 s and a total printing time of 310 min.

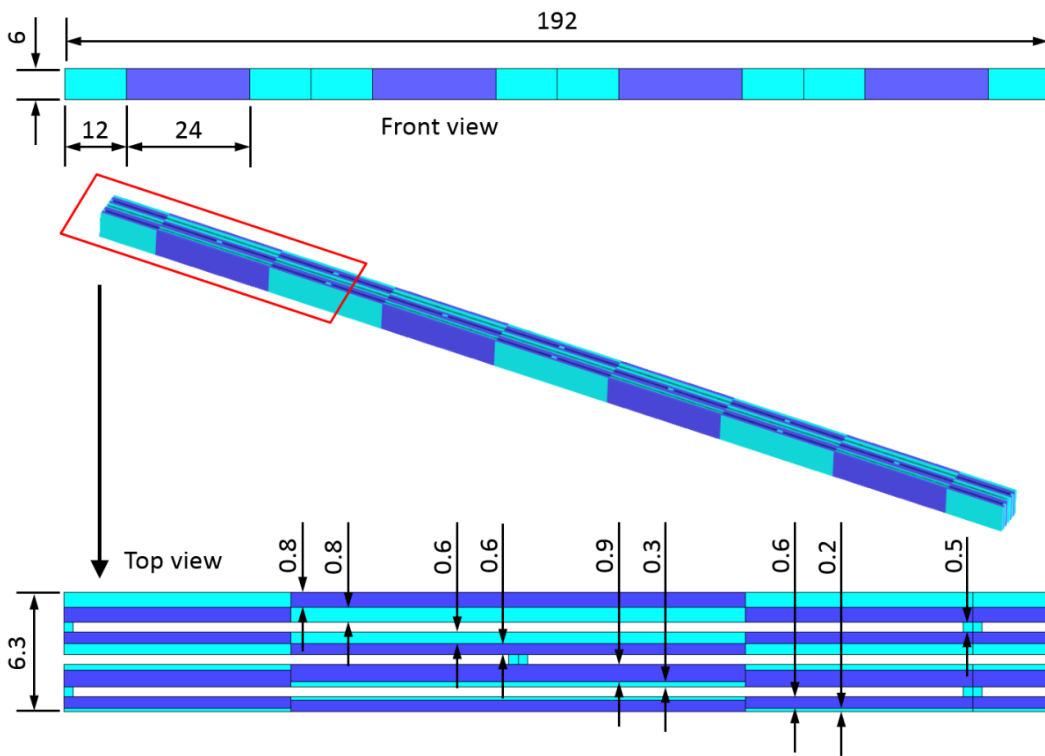


**fig. S8. Design of the printed sample in Fig. 4B.** Closed lattice with an overall size of 192 mm  $\times$  6.3 mm  $\times$  6 mm. Veroclear/Tangoblack bilayers are printed perpendicular to the build tray, have a series of thicknesses of 0.8/0.8, 0.6/0.6, 0.3/0.9, and 0.2/0.6 mm, and are fabricated with a layer printing time of 68 s and a total printing time of 273 min.

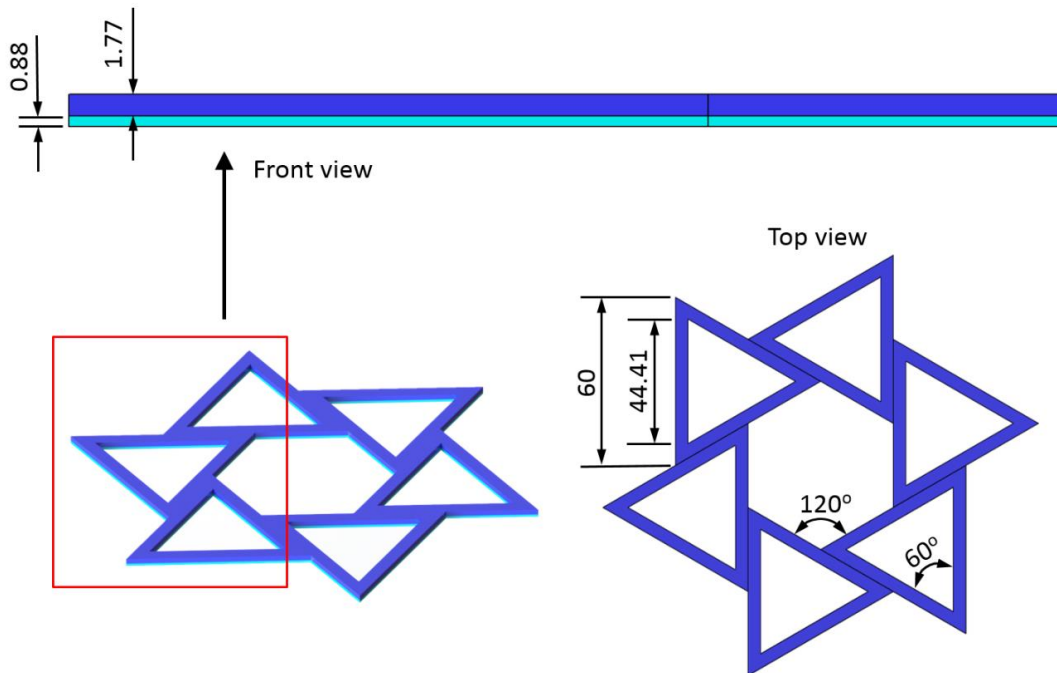


**fig. S9. Design of the printed sample in Fig. 4C.** Flat star-shaped bilayer structure consists of 6 identical equilateral triangles, each of which has outer/inner side length of 60/44.41 mm. The

Veroclear/Tangoblack+ thicknesses are 0.88/1.77 mm and the structure is fabricated with a layer printing time of 68 s and a total printing time of 144 min.

For Fig. 4D, printed flower consisting of five layers of petals with a gap of 0.5 mm between each. The petals in different layers are similar in shape and size, except for the outer radius (42, 48, and 51 mm). Each petal is a flat bilayer structure, and has a SMP/elastomer thicknesses of 0.3/0.3 mm. The maximum petal width is less than 4.5 mm. The elastomer is Tango+, while SMP is the digital materials/composites from Pureverowhite, Veroyellow, Veromagenta, Veroblack and Verocyan. The printing time for petals from the bottom layer to top layer is 25, 37, 49, 58 and 74 s, respectively, and the total printing time for the flower is 352 min. Unlike the other samples, the flower is printed on the Stratasys J750 multimaterial printer which supports the multiple color materials.

In fig. S1, flat strips of  $\sim 20 \text{ mm} \times 7 \text{ mm} \times 1 \text{ mm}$  (Veroclear and Tangoblack+) for storage modulus/glass transition measurements and  $\sim 25 \text{ mm} \times 8 \text{ mm} \times 0.6 \text{ mm}$  for thermal strain measurements. These samples are fabricated with a layer printing time of 68 s and the total printing time of 82 min for the former and 66 min for the latter.



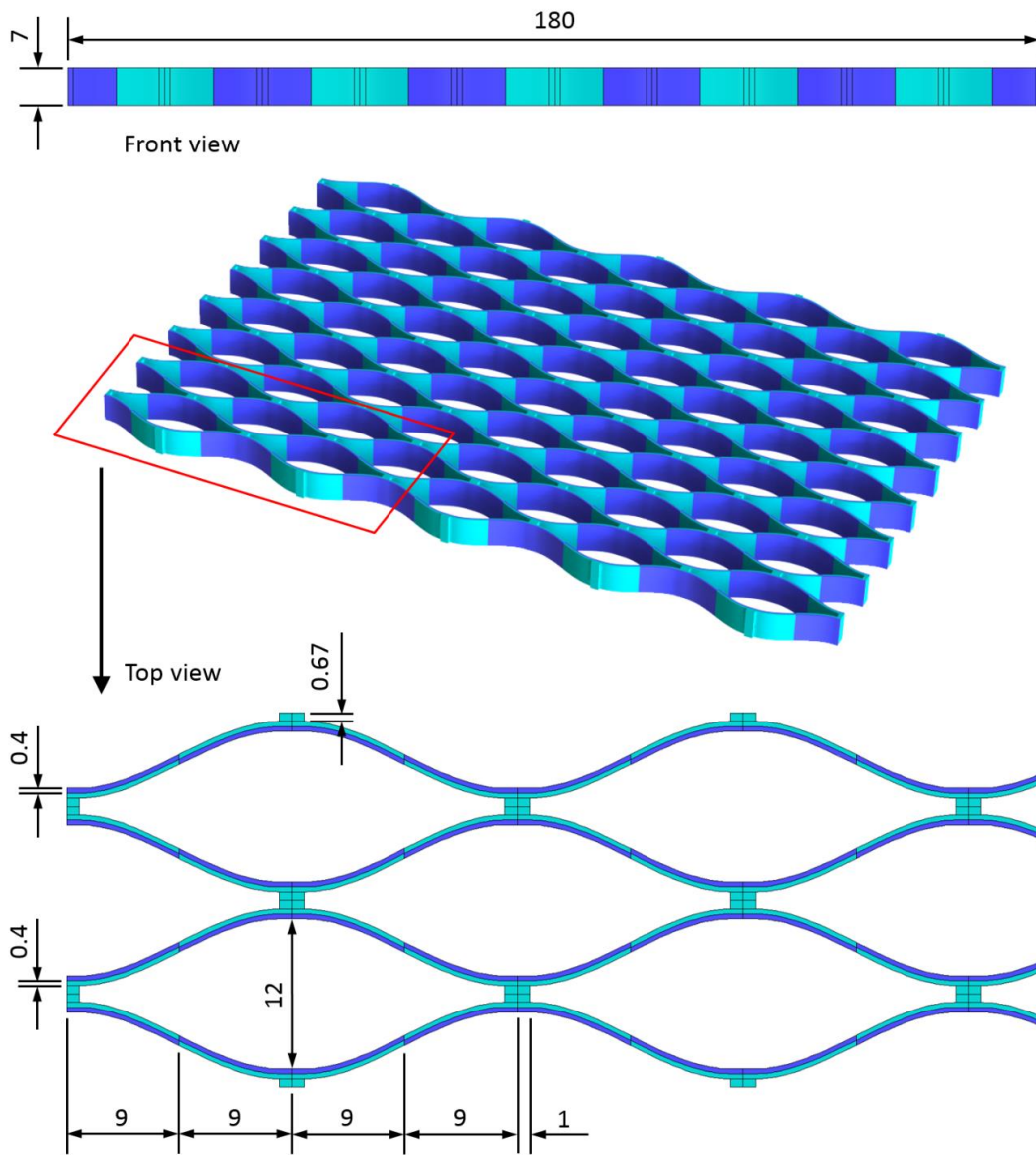


**fig. S10. Design of the printed sample in fig. S3.** Open lattice with an overall size of 180 mm  $\times$  119 mm  $\times$  7 mm. Veroclear/Tangoblack bilayers are printed perpendicular to the build tray, have a thicknesses of 0.4/0.4 mm, and are fabricated with a layer printing time of 68 s and a total printing time of 310 min.

#### section S4. Modeling and simulation

In order to describe the shape change behavior of the printed structures and reveal its mechanism, we build a model that accounts for the temperature-dependent thermomechanical behavior of SMP material and the experimentally-determined built-in compressive strain in the elastomer. Multibranch model is used to describe the thermomechanical property of SMP material, in which one equilibrium branch and several thermoviscoelastic nonequilibrium branches are arranged in parallel (24). Maxwell elements are used in the nonequilibrium branches to represent the stress relaxation behavior of the material, and the total stress of the SMP material can be expressed as

$$\sigma_s = E_s^{eq} e_s + \sum_{m=1}^n E_m^{non} \int_0^t \frac{\partial e_s}{\partial s} \exp \left[ -\int_s^t \frac{dt'}{\tau_m(T)} \right] ds \quad (S1)$$

Where  $E_s^{eq}$  is the elastic modulus of the equilibrium branch,  $E_m^{non}$  and  $\tau_m$  are the elastic modulus and temperature dependent relaxation time of the  $m^{\text{th}}$  nonequilibrium branch,  $e_s$  is the mechanical strain calculated by subtracting the thermal strain  $\alpha_s \Delta T$  from total strain.

Based on the time temperature superposition principle (TTSP),  $\tau_m$  can be determined by using the relaxation time  $\tau_m^R$  at reference temperature

$$\tau_m(T) = a^{shift}(T) \tau_m^R \quad (S2)$$

where  $a^{shift}(T)$  is the temperature dependent shifting factor. The shifting factors can be calculated by combining the Williams–Landel–Ferry (WLF) equation and Arrhenius-type equation (24). When the temperature is higher than the reference temperature  $T_{ref}$ , the shifting factor can be expressed by using WLF equation

$$\log \left[ a^{shift}(T) \right] = -\frac{C_1 (T - T_{ref})}{C_2 + (T - T_{ref})}, T > T_{ref} \quad (S3)$$

where  $C_1$ ,  $C_2$  and  $T_{ref}$  are the material parameters to be characterized. If the temperature is lower than the reference temperature  $T_{ref}$ , the shifting factor can be expressed by Arrhenius-type equation: (S1)

$$\ln \left[ a^{shift}(T) \right] = -\frac{AF_c}{k} \left( \frac{1}{T} - \frac{1}{T_{ref}} \right), T < T_{ref} \quad (S4)$$

where  $A$ ,  $F_c$  and  $k$  are the material constant, configurational energy and Boltzmann's constant respectively.

The DMA test results in the Supplementary Information were used to identify the above parameters including  $E_s^{eq}$ ,  $E_m^{non}$ ,  $\tau_m^R$ ,  $C_1$ ,  $C_2$  and  $AF_c/k$ . The storage modulus at 80°C can be considered as the equilibrium modulus  $E_s^{eq}$  as the relaxation time at this temperature in each nonequilibrium branch is minimal.

For the multi-branch linear model, the temperature dependent storage modulus  $E_s(T)$ , loss modulus  $E_l(T)$  and loss factor  $\tan \delta$  can be respectively represented as

$$E_s(T) = E_{eq} + \sum_{m=1}^n \frac{E_m^{non} \omega^2 [\tau_m(T)]^2}{1 + \omega^2 [\tau_m(T)]^2} \quad (S5A)$$

$$E_l(T) = \sum_{m=1}^n \frac{E_m^{non} \omega \tau_m(T)}{1 + \omega^2 [\tau_m(T)]^2} \quad (\text{S5B})$$

$$\tan \delta = \frac{E_l(T)}{E_s(T)} \quad (\text{S5C})$$

where  $\omega$  is the test frequency. Employing the nonlinear regression (NLREG) method (24),  $E_m^{non}$ ,  $\tau_m^R$ ,  $C_1$ ,  $C_2$  and  $AF/k$  can be determined by fitting the storage modulus and  $\tan \delta$  curves shown in fig. S1A and B. The fitted parameters are listed in table S1.

For the elastomer, it is seen from fig. S1A that the storage modulus is almost temperature-independent above room temperature. So for simplicity, a linear elastic model is used to describe the rubber material

$$\sigma_{elas}(y) = E_{elas} \left( e_{elas}^{total} - e_{elas}^{thermal} - e_{elas}^{printing} \right), \quad (\text{S6})$$

where  $E_{elas}$  is the elastic modulus and  $e_{elas}^{total}$ ,  $e_{elas}^{thermal}$ ,  $e_{elas}^{printing}$  are the total strain, thermal strain ( $\alpha_{elas} \Delta T$ ) and printing bulid-in strain of the elastomer, respectively.

**table S1. List of parameters for constitutive model.**

Branch	$E^{non}$ (Pa)	$\tau^R$ (s)	Branch	$E^{non}$ (Pa)	$\tau^R$ (s)
1	1.49E+08	2.00E-08	15	1.42E+08	927.9366
2	1.2E+08	4.27E-07	16	1.12E+08	8849.219
3	1.32E+08	5.47E-06	17	1.41E+08	2849.202
4	1.47E+08	5.89E-05	18	81897206	25294.7
5	1.66E+08	0.000547	19	52681974	7.29E+04
6	1.89E+08	0.004524	20	12478539	653520.3
7	2.08E+08	0.032439	21	28031731	2.13E+05
8	2.51E+08	0.2	22	1712558	5.37E+06
9	1.78E+08	1	23	4830405	2000000
10	1.44E+08	3.250259	24	1197657	8.54E+07
11	1.51E+08	9.451896	25	1383214	2.00E+07
12	1.63E+08	30.23741	26	182.666	3.61E+08
13	1.62E+08	100	27	2537188	2.00E+09
14	1.51E+08	315.2367			
$E_S^{eq}$ (Pa)	6E+06		AF <sub>c</sub> /k		-24000
$C_1$	17.4		$T_{ref}$ (°C)		22
$C_2$	66.35		$\alpha_S$ (/°C)		1.7E-4
$E_{elas}$ (Pa)	0.6E+06		$\alpha_{elas}$ (/°C)		2.3E-4